SLEEPJ, 2021, 1–12

doi: 10.1093/sleep/zsaa199
Advance Access Publication Date: 25 September 2020
Original Article

ORIGINAL ARTICLE

Convergent patterns of structural brain changes in rapid eye movement sleep behavior disorder and Parkinson's disease on behalf of the German rapid eye movement sleep behavior disorder study group

Florian Holtbernd[1,2,3,*], Sandro Romanzetti[1,2,*], Wolfgang Hermann Oertel[4], Susanne Knake[4,5], Elisabeth Sittig[4], Anna Heidbreder[6,7], Andrea Maier[1], Janna Krahe[1,2], Jennifer Wojtala[1,2], Imis Dogan[1,2], Jörg Bernhard Schulz[1,2], Johannes Schiefer[1], Annette Janzen[4,§] and Kathrin Reetz[1,2,†,§]; on behalf of the German RBD Study Group

[1]Department of Neurology, RWTH Aachen University, Aachen, Germany, [2]JARA-BRAIN Institute Molecular Neuroscience and Neuroimaging, Juelich Research Center GmbH and RWTH Aachen University, Aachen, Germany, [3]Institute of Neuroscience and Medicine 4 (INM-4), Juelich Research Center, Juelich, Germany, [4]Department of Neurology, Philipps-University Marburg, Marburg, Germany, [5]CMBB, Center for Mind, Brain and Behavior, University Hospital Marburg, Marburg, Germany, [6]Department of Neurology with Institute of Translational Neurology, University Hospital Muenster, Muenster, Germany and [7]Department of Neurology, Medical University Innsbruck, Innsbruck, Austria

[†]Corresponding author. Kathrin Reetz, Department of Neurology, University Clinic Aachen, Pauwelsstr. 30, 52074 Aachen, Germany. Email: kreetz@ukaachen.de.

[*]These authors contributed equally to this work.

[§]These authors shared senior authorship.

Abstract

Study Objectives: Rapid eye movement sleep behavior disorder (RBD) is considered a prodromal state of Parkinson's disease (PD). We aimed to characterize patterns of structural brain changes in RBD and PD patients using multimodal MRI.

Methods: A total of 30 patients with isolated RBD, 29 patients with PD, and 56 age-matched healthy controls (HC) underwent MRI at 3T, including tensor-based morphometry, diffusion tensor imaging, and assessment of cortical thickness.

Results: RBD individuals showed increased volume of the right caudate nucleus compared with HC, and higher cerebellar volume compared with both PD subjects and HC. Similar to PD subjects, RBD patients displayed increased fractional anisotropy (FA) in the corticospinal tracts, several tracts mainly related to non-motor function, and reduced FA of the corpus callosum compared with HC. Further, RBD subjects showed higher FA in the cerebellar peduncles and brainstem compared with both, PD patients and HC. PD individuals exhibited lower than normal volume in the basal ganglia, midbrain, pedunculopontine nuclei, and cerebellum. In contrast, volume in PD subjects was increased in the thalamus compared with both HC and RBD subjects.

Conclusions: We found convergent patterns of structural brain alterations in RBD and PD patients compared with HC. The changes observed suggest a co-occurrence of neurodegeneration and compensatory mechanisms that fail with emerging PD pathology. Our findings strengthen the hypothesis of RBD and PD constituting a continuous disease spectrum.

Statement of Significance

Rapid eye movement sleep behavior disorder (RBD) heralds the subsequent development of Parkinson's disease (PD) and other alpha-synucleinopathies. Epidemiological studies suggest a neurodegenerative disease risk of 70%–75% over a 12-year period in RBD individuals. In this multicenter, multimodal MRI study, we demonstrate convergent patterns of structural and microstructural brain alterations in RBD and PD. The presence of bidirectional changes of the structural integrity in multiple brain regions, including, but not limited to those commonly associated with RBD and PD pathophysiology, suggests a co-occurrence of compensatory and neurodegenerative mechanisms. This study supports the hypothesis of RBD and PD representing aspects of a continuous disease spectrum, and contributes to a better understanding of their pathophysiological relationship.

Key words: MRI; Parkinson's disease; RBD; REM sleep behavior disorder; prodromal

Submitted: 26 March, 2020; **Revised:** 8 September, 2020

Introduction

Rapid eye movement sleep behavior disorder (RBD) is characterized by the enactment of, often vivid, dreams accompanied by a loss of muscle atonia during rapid eye movement sleep on polysomnography [1]. RBD is strongly associated with the subsequent development of alpha-synucleinopathies such as dementia with Lewy bodies, multiple system atrophy, and particularly, Parkinson's disease (PD). Indeed, evidence from epidemiological studies suggests that conversion rates to alpha-synucleinopathies may be as high as 73% over a 12 year period [2]. It remains unclear, however, why some cases of clinically isolated RBD without any motor or cognitive manifestations of PD do not continue to eventually develop progressive neurodegenerative disease. Moreover, some individuals who never experienced rapid eye movement sleep abnormalities develop RBD only years after they have been diagnosed with PD, challenging the concept of RBD unequivocally reflecting a prodromal state of alpha-synucleinopathies [3]. That being said, there is mounting evidence from neuroimaging studies indicating a substantial pathophysiological overlap between RBD and PD [4]. Striatal dopamine levels have consistently been found to be reduced in RBD [5], and RBD patients exhibit metabolic brain changes that resemble those typically seen in PD [6, 7]. In line with histopathological findings, reduced structural integrity on conventional and diffusion tensor imaging (DTI) MRI has been reported in the brainstem (BS) and midbrain of RBD patients [8, 9]. Findings on structural abnormalities in other subcortical and cortical regions are less consistent. Scherfler et al. [8] found an increased gray matter volume in the hippocampus, others reported reductions of brain tissue volume in parahippocampal regions, putamen, and cerebellum (CER) in RBD patients [10, 11]. However, studies directly comparing structural brain alterations in combined cohorts of RBD and PD patients are scarce. Here, we aimed to explore whether RBD and PD patients shared overlapping patterns of structural brain alterations using multimodal MRI.

Methods

Subjects

For this retrospective, cross-sectional study, RBD and PD subjects and age-matched HC were recruited at the movement disorder and sleep clinics at the universities of Aachen and Marburg, Germany. In addition, demographical and MRI data from eligible subjects classified as RBD archived in the Parkinson's Progression Markers Initiative (PPMI) database were extracted (www.ppmi-info.com; last database query on 06/18). PD subjects were diagnosed according to the UK Parkinson's disease society brain bank diagnostic criteria [12]. All RBD cases were confirmed by polysomnography in line with the criteria proposed by the American Academy of Sleep Medicine [13]. The presence of RBD was not assessed in the PD cohort. Exclusion criteria were the presence of concurrent relevant neurological diseases, cognitive impairment (defined as a Montreal Cognitive Assessment (MoCA) [14] score <25), and overt motor symptoms likely to be attributable to PD in RBD individuals (defined as a Unified Parkinson's disease Rating Scale [15] [UPDRS] part III score >5). The levodopa equivalent daily dosage (LEDD) was calculated for each individual. UPDRS III motor scores were used to determine the more severely affected body side, and the motor phenotype (tremor dominant or akinetic rigid) was assessed according to a previously published method [16]. One patient in the Marburg RBD cohort received 0.7 mg pramipexole daily because of concurrent restless legs syndrome, and another RBD subject from the same cohort was treated with low dose rotigotine (4 mg daily) for refractory RBD symptoms. In total, 30 RBD individuals (age: 66.8 ± 9.1 years, 1 female), 29 PD patients (age: 63.5 ± 8.3, 8 females), and 56 age-matched HC (age: 62.9 ± 11.0, 14 females) were included. Due to the retrospective nature of this study and typically very low number of females in the RBD cohort, we were not able to achieve a perfect matching of gender between the HC and both the RBD and PD cohorts, respectively. As it was our primary hypothesis that RBD constitutes a prodromal state of PD, we decided to match the HC cohort to the PD cohort with respect to gender. The study was conducted according to the Declaration of Helsinki and written informed consent was obtained from each participant. The study has been approved by the local ethics committees at Aachen (EK 231/09) and Marburg (AZ 89/12) universities, respectively. The demographical and clinical data are detailed in Table 1.

Motor and cognitive assessments

Standardized motor and cognitive assessments were applied using the UPDRS part III and MoCA. For RBD subjects obtained from the PPMI database, the revised MDS-UPDRS [17] part III was used. For four subjects (three HC and one RBD subject), no MoCA was available, and the Mini-Mental-State Examination (MMSE) [18] score was used instead.

Magnetic resonance imaging

All subjects underwent high-resolution T1 weighted MRI at 3T. A total of 99 of the 115 subjects (53 HC, 23 RBD, and 23 PD) were available for additional DTI. Subjects obtained from the PPMI database were scanned according to the published protocol (available at https://www.ppmi-info.org/study-design/research-documents-and-sops/). MRI imaging at the university of Marburg was performed on a 3T TIM Trio scanner. Subjects recruited in Aachen were scanned on a 3T Prisma (N = 57) or on a 3T TIM Trio (N = 22) scanner, respectively. All scanners were manufactured by Siemens (Siemens Healthlineers, Erlangen, Germany). The MRI acquisition details are presented in Supplementary Table S1.

Morphological analysis

Anatomical images were analyzed with the Advanced Normalization Tools (ANTs) software package (Version 2.1.1; http://stnava.github.io/ANTs/). A freely available brain template based on a subset of the OASIS public neuroimaging datasets [19] was used for all analyses in this study (including DTI). The template is pre-segmented into the following regions of interest (ROI): cortical gray matter, white matter, deep gray matter (DGM), CER, and BS. Images of the brain of each subject were normalized to the study template by running the *antsCorticalThickness.sh* script provided with the ANTs package. In addition to the normalization, the script generates the following datasets: cortical thickness (CT) maps in

Table 1. Summary of demographical and clinical data

	HC			RBD				PD		
Site	Marburg (n = 10)	Aachen (n = 46)	Total (n = 56)	Marburg (n = 8)	Aachen (n = 14)	PPMI (n = 8)	Total (n = 30)	Marburg (n = 10)	Aachen (n = 19)	Total (n = 29)
Gender	3f/7m	11f/35m	14f/42m	1f/7m	14m	8m	1f/29m	1f/9m	7f/12m	8f/21m
Age (years)	66.5 ± 14.3 (30–77)	62.2 ± 10.1 (31–81)	62.9 ± 11.0 (30–81)	67.1 ± 6.4 (61–77)	64.9 ± 11.7 (32–78)	70.3 ± 5.7 (63–81)	66.8 ± 9.1 (32–81)	61.1 ± 9.5 (47–76)	64.7 ± 7.6 (47–76)	63.5 ± 8.3 (47–76)
UPDRS III	0.6 ± 1.3 (0–4)	0.3 ± 0.7 (0–3)	0.4 ± 0.8 (0–4)	1.6 ± 1.7 (0–4)	2.4 ± 2.0 (0–5)	2.8 ± 1.4* (0–5)	2.3 ± 1.8 (0–5)	15.7 ± 6.1 (8–26)	24.3 ± 10.0 (10–47)	21.3 ± 9.7 (8–47)
Disease duration (months)	n/a	n/a	n/a	42.0 ± 27.2(9–84)	147.7 ± 213.3 (12–708)	146.9 ± 121.4 (6–364)	121.0 ± 162.4† (6–708)	22.6 ± 14.5 (8–48)	102.4 ± 91.1 (9–369)	80.9 ± 85.7‡ (8–369)
MoCA	28.0 ± 1.3 (26–30)	28.3 ± 1.4 (25–30)	28.3 ± 1.4§ (25–30)	28.4 ± 1.6 (25–30)	28.0 ± 1.4 (25–30)	28.0 ± 1.9 (25–30)	28.1 ± 1.5§ (25–30)	28.1 ± 1.3 (26–30)	28.1 ± 1.3 (26–30)	28.1 ± 1.3 (26–30)
H&Y	n/a	n/a	n/a	n/a	n/a	n/a	n/a	1.7 ± 0.7 (1–3)	1.9 ± 0.7 (1–3)	1.8 ± 0.7 (1–3)
LEDD (mg)	0	0	0	18.8 ± 37.2 (50–100)	0	0	5.0 ± 20.1 (50–100)	120.0 ± 145.7 (0–450)	541.2 ± 389.7 (0–1,550.8)	395.9 ± 382.1 (0–1,550.8)
Laterality of motor symptoms	n/a	n/a	n/a	n/a	n/a	n/a	n/a	3 left/7 right	6 left/13 right	9 left/ 20 right
PD subtype								6 AR/ 3 TR/1MI	11 AR/8 TR	17 AR/ 11 TR/ 1MI

HC, healthy control; RBD, REM sleep behavior disorder; PD, Parkinson's disease; PPMI, Parkinson's progression markers initiative; UPDRS, Unified Parkinson's Disease rating scale; MoCA, Montreal cognitive assessment; H&Y, Hoehn and Yahr; LEDD, Levodopa equivalent daily dosage; AR, akinetic-rigid; TR, tremor dominant; MI, mixed type; n/a, not applicable. Values are presented as mean ± SD (range).

*Movement disorder society (MDS)-UDPRS.

†Data missing for 2 individuals (1 from Marburg and 1 from Aachen).

‡Data missing for 3 individuals (all from Marburg).

§MMSE was used instead of MoCA in 3 HC (all from Aachen) and 1 RBD individual (Aachen).

the anatomical coordinates of the subjects and of the template, geometrical transformations to map images from the subject's space to the template space, and their log-Jacobian. A detailed description of the script has been published previously [20].

Tensor-based morphometry

Tensor-based morphometry (TBM) uses the nonlinear transformations that aligned each individual brain to the template as basis for quantification. Specifically, this is done by using the logarithm of the Jacobian determinant of each transformation, which represents local volume expansions ($\log(\nabla J) < 0$), or contractions ($\log(\nabla J) > 0$) as compared with the normalizing template [21]. Since the log-Jacobian maps were all defined in the same anatomical coordinates delineated by the template, systematic group changes were analyzed for each ROI defined in template space utilizing a voxelwise statistical approach.

Cortical thickness

To analyze differences in CT across groups, we performed voxelwise permutation tests on the CT datasets projected to the coordinates of the template. The permutation tests were run exclusively on cortical gray matter regions.

Diffusion tensor imaging

Diffusion weighted images (DWI) were analyzed with the MrTrix software package (version RC3-159-gdfda38fd). After denoising, image distortions determined by eddy-currents and susceptibility effects were corrected by normalizing each DWI dataset to the corresponding subject's T1 image through a rigid transformation followed by a nonlinear transformation (i.e. SyN [20]). Furthermore, each dataset was resized to have a common spacing, defined as the lowest among all the available datasets (2.4 mm). After preprocessing, the following DTI parameters were calculated from each dataset: fractional anisotropy (FA), mean diffusivity (MD), radial diffusivity (RD), and axial diffusivity (AD). Finally, each diffusion measure was mapped to the template space. This was performed by: (1) finding the optimal rigid and nonlinear transformations that mapped the FA datasets to the subject's white matter obtained by masking the subject's T1 image and (2) by combining these with the transformations that mapped the subject's T1 images to the template [22]. The resulting combined transformations were used to project the FA (threshold >0.2), MD, RD, and AD maps to the template space. In a similar fashion as for the statistical analysis of the CT and TBM data, we used permutation tests to find significant changes in DTI measures across groups. DTI measures were analyzed in the same ROIs as described in the TBM analysis.

Statistical analyses

All voxelwise permutation tests were performed with the command line tool Randomise Group Level included in the BROCCOLI software [23]. In each case, 10,000 permutations were performed at a significance level of $p < 0.05$. We first performed an ANOVA in each ROI specified above to search for significant differences across the three groups (HC, RBD, and PD). The ANOVA was based on a permutation test which resulted in f-value and p-values

maps for each ROI. A cluster interference mode with an f-value threshold of 2.5 was used to identify regions of significant difference among groups. Age, gender, and site of imaging were entered as nuisance variables in all analyses. For exact anatomical allocation of statistically significant clusters found within each ROI, we utilized three atlases: the JHU DTI white matter atlas [24], the SUIT cerebellar atlas [25], and a lab-made atlas, which incorporated two previously published MRI atlases [26, 27], including nuclei relevant to RBD pathophysiology. The ANOVA indicated voxels showing significantly different values across groups, but did not specify which of the three groups differed from one another in a given voxel, or the nature of the differences observed (i.e. which group showed higher or lower values, respectively). Thus, we performed post hoc t-tests (HC vs. PD, HC vs. RBD, HC vs. PD) with Bonferroni corrections for multiple testing by extracting the individual values of all significant voxels allocated to one of the atlas-based anatomically defined regions within each of the ROIs. Only anatomical regions containing at least 5% of significant voxels were included in the post hoc analyses. For comparisons of demographical data, one-way ANOVA with post hoc Bonferroni corrections for multiple comparisons and the chi-squared test were applied where appropriate. The Pearson correlation coefficient was used for correlational analysis of behavioral data with regional values of significant clusters. Statistical analyses were performed in SPSS 25 and R (http://www.R-project.org/). Results were deemed significant at $p < 0.05$.

Results

Demographics and clinical data

Age and cognitive status did not differ across the three groups (age: $F_{(2,114)} = 1.561$, $p = 0.214$; MoCA: $F_{(2,114)} = 0.302$, $p = 0.740$). There was a lower number of females in the RBD cohort compared with both the HC cohort ($X^2 = (1, n = 86) = 6.369$, $p < 0.02$) and PD group ($X^2 = (1, n = 56) = 6.709$, $p < 0.01$). There was no difference in gender distribution in the PD compared with the HC cohort ($X^2 = (1, n = 86) = 0.067$, $p = 0.796$).

Magnetic resonance imaging

Brain regions exhibiting significant differences across the three groups and the corresponding post hoc statistics of the regional values are summarized in Table 2. We also included the effect sizes of significant clusters identified in the TBM analyses (Supplementary Table S2).

Tensor-based morphometry

We found significant differences of brain volume across the three groups (HC, RBD, and PD) in the DGM ROI (Figure 1, A). Post hoc testing revealed increased volume of the right caudate nucleus in RBD individuals compared with HC ($p < 0.04$, Figure 2, A). PD patients showed higher volume compared with both HC and RBD patients in the bilateral thalamus ($p < 0.004$ and $p < 0.05$, respectively, Figure 2, B and C). In contrast, compared with HC, PD patients exhibited lower volume in the substantia nigra ($p < 0.03$), bilateral putamen, and globus pallidum ($p < 0.03$ for all, Figure 2, D).

In the BS ROI, significantly different brain volume across groups was apparent in the medulla oblongata, pons, locus coeruleus (LC), pedunculopontine nuclei (PPN), and red nuclei (Figure 1, B). Post hoc pairwise comparisons revealed higher volume in RBD patients compared with PD in the LC, medulla oblongata, including the medullary reticularis formation (MRF), and pons ($p < 0.05$ for all, Figure 2, E). There was a trend toward higher pontine volume in RBD patients compared with HC in the latter region ($p = 0.056$). PD individuals showed lower than normal volume of the PPN ($p < 0.04$, Figure 2, F), and a trend level reduction in the LC ($p = 0.058$).

Additional significant differences of volume across groups were observed in the cerebellar ROI (Figure 1, C). Post hoc tests showed larger cerebellar volume in RBD subjects compared with HC in the Crus I, lobule X, and cerebellar white matter ($p < 0.04$ for all, Figure 2, G). There also were widespread volume increases in RBD individuals compared with their PD counterparts in the anterior and posterior CER, including lobules I–V, VIIb, VIIIa/b, IX, X, Crus I, and cerebellar white matter, extending to the cerebellar peduncles ($p < 0.05$ for all, Figure 2, H). In contrast, PD patients displayed lower volume compared with HC in lobules I–IV, Crus II, VIIb, and VIIIa/b ($p < 0.05$ for all, Figure 2, I).

Cortical thickness

We did not observe any significant differences of CT across groups.

Diffusion tensor imaging

We found widespread alterations of FA across groups in the BS ROI (Figure 3, A), cerebellar ROI (Figure 3, B), and white matter ROI (Figure 3, C and D).

Post hoc tests revealed higher FA in RBD subjects compared with HC in the bilateral substantia nigra, bilateral red nuclei, PPN, dorsal and medial raphe nuclei, LC, and the medulla oblongata, including the MRF ($p < 0.04$ for all, Figure 4, A). With the exception of the left red nucleus and the MRF, RBD subjects also showed higher FA values in the latter regions compared with PD subjects ($p < 0.05$ for all, Figure 4, B). Moreover, RBD individuals showed abnormally elevated FA compared with HC in the bilateral inferior, middle, and superior cerebellar peduncles ($p < 0.005$ for all, Figure 4, C), and higher FA compared with the PD group in both superior cerebellar peduncles, and the right inferior cerebellar peduncle ($p < 0.04$ for all, Figure 4, D). Compared with HC, both RBD and PD individuals displayed lower FA in the corpus callosum ($p < 0.003$ and $p < 0.02$, respectively, Figure 4, E and F). In contrast, RBD subjects displayed higher than normal FA in both corticospinal tracts, right superior longitudinal fasciculus, right anterior thalamic radiation, and the left uncinate fasciculus ($p < 0.02$ for all, Figure 4, G). Similarly, PD patients showed elevated FA compared with HC in the right corticospinal tract, right longitudinal fasciculus, and right uncinate fasciculus ($p < 0.04$ for all, Figure 4, I). Analysis of the MD, RD, and AD did not reveal significant differences across groups.

Correlation of MRI measures with motor severity

To investigate the relationship of the brain structural alterations with motor dysfunction, we performed additional correlational analyses of TBM and FA measures with motor UPDRS scores. As defined by the inclusion criteria, only PD individuals exhibited a

Table 2. Results of post hoc analyses of significant clusters

Region	HC (mean ± *SD*)	RBD (mean ± *SD*)	PD (mean ± *SD*)	Cluster (voxel)	ROI (voxel)	Ratio (%)	*P* (corrected) PD vs. HC	RBD vs. HC	RBD vs. PD
TBM (Log-Jacobian) DGM and BS									
L Globus pallidum	−6.57 ± 10.76	−7.89 ± 9.15	−12.40 ± 8.12	67	155	43	**0.020**	0.999	0.150
L Putamen	−14.06 ± 10.69	−16.08 ± 10.76	−20.69 ± 7.85	159	444	36	**0.005**	0.999	0.194
L Thalamus	−4.22 ± 6.87	−3.57 ± 7.29	3.29 ± 9.47	367	988	37	**0.001**	0.999	**0.009**
L Substantia nigra	−9.63 ± 9.83	−11.07 ± 7.29	−15.57 ± 8.95	35	58	60	**0.024**	0.999	0.115
L/R Pendunculopontine Nucleus	−6.60 ± 9.57	−7.30 ± 8.22	−12.05 ± 8.33	29	59	49	**0.034**	0.999	0.094
L/R Locus coeruleus	−1.61 ± 8.12	−1.27 ± 6.72	−5.92 ± 7.45	18	35	51	0.058	0.999	**0.044**
L/R Medulla oblongata	11.53 ± 9.28	14.39 ± 9.33	7.74 ± 9.82	410	598	69	0.250	0.534	**0.030**
L/R medullary reticularis formation	−5.29 ± 9.82	−3.76 ± 7.74	−9.36 ± 8.05	23	25	92	0.174	0.999	**0.026**
L/R Pons	−4.60 ± 10.16	0.71 ± 8.99	−6.68 ± 10.48	505	983	51	0.999	0.056	**0.015**
R Globus pallidum	−8.10 ± 9.26	−11.56 ± 9.20	−13.16 ± 6.96	48	157	31	**0.018**	0.309	0.999
R Putamen	−12.21 ± 9.97	−15.73 ± 8.41	−19.15 ± 6.75	328	441	74	**0.001**	0.264	0.269
R Thalamus	−4.23 ± 7.18	−2.35 ± 6.14	3.03 ± 9.73	279	933	30	**0.003**	0.624	**0.045**
R Caudate	11.31 ± 16.87	21.18 ± 16.31	19.78 ± 27.15	189	403	47	0.399	**0.031**	0.999
R Substantia nigra	−8.10 ± 9.38	−9.18 ± 7.22	−13.90 ± 7.83	50	60	83	**0.016**	0.999	0.058
TBM (Log-Jacobian) CER									
L Crus I	−11.40 ± 12.23	−3.59 ± 9.21	−11.70 ± 12.67	291	1,723	17	0.999	**0.004**	**0.021**
L Crus II	−7.46 ± 10.41	−7.12 ± 12.04	−14.95 ± 12.72	610	1,335	46	**0.026**	0.999	0.056
L I–IV	−1.15 ± 9.13	0.30 ± 9.29	−7.84 ± 11.41	201	418	48	**0.026**	0.999	**0.012**
L IX	−2.51 ± 10.70	3.83 ± 13.90	−5.63 ± 13.76	166	446	37	0.873	0.104	**0.033**
L V	−1.92 ± 14.78	0.81 ± 12.51	−8.88 ± 14.77	76	566	13	0.132	0.999	**0.026**
L VIIb	−5.51 ± 9.63	−6.37 ± 11.08	−12.03 ± 10.35	259	640	40	**0.020**	0.999	0.142
L VIIIa	−0.21 ± 11.95	−4.01 ± 13.22	−9.05 ± 13.16	73	638	11	**0.011**	0.585	0.444
L VIIIb	−1.98 ± 11.46	2.17 ± 10.75	−7.96 ± 12.10	111	540	21	0.096	0.999	**0.004**
L X	16.04 ± 11.18	21.41 ± 9.52	13.35 ± 11.65	6	60	10	0.936	0.066	**0.016**
White matter	−7.36 ± 8.63	−1.08 ± 8.35	−8.25 ± 6.89	850	1,768	48	0.999	**0.005**	**0.002**
Vermis Crus II	6.14 ± 15.52	4.57 ± 15.75	−3.06 ± 15.15	12	58	21	**0.032**	0.999	0.189
Vermis IX	−7.20 ± 10.88	−4.17 ± 13.22	−11.86 ± 10.33	47	100	47	0.172	0.861	**0.047**
Vermis VIIIa	−1.10 ± 9.93	−2.71 ± 13.39	−7.65 ± 8.86	15	159	9	**0.009**	0.999	0.299
Vermis VIIIb	−5.68 ± 11.21	−6.35 ± 12.32	−12.13 ± 9.21	35	89	39	**0.018**	0.999	0.137
R Crus I	−3.35 ± 12.18	2.63 ± 9.11	−6.28 ± 11.58	480	1,774	27	0.846	**0.037**	**0.006**
R Crus II	−0.40 ± 11.48	−4.37 ± 13.07	−11.06 ± 15.42	536	1,216	44	**0.006**	0.501	0.236
R I–IV	0.18 ± 12.58	−2.98 ± 13.86	−9.70 ± 12.83	58	527	11	**0.004**	0.912	0.175
R VIIb	−4.08 ± 9.11	−4.43 ± 8.28	−10.01 ± 8.47	273	739	37	**0.012**	0.999	**0.040**
R VIIIa	−4.02 ± 8.71	−1.32 ± 7.40	−10.17 ± 8.82	342	620	55	**0.010**	0.408	**0.001**
R VIIIb	−0.23 ± 10.00	4.99 ± 11.86	−5.24 ± 11.37	225	505	45	0.151	0.136	**0.004**
R X	13.67 ± 11.55	20.83 ± 9.19	11.16 ± 13.64	24	63	38	0.999	**0.007**	**0.008**
FA BS and midbrain									
L Red nucleus	0.32 ± 0.07	0.37 ± 0.07	0.32 ± 0.07	9	62	15	0.999	**0.030**	0.074
L Substantia nigra	0.42 ± 0.07	0.48 ± 0.07	0.42 ± 0.08	4	58	7	0.999	**0.005**	**0.030**
L/R Median raphe nuclei	0.24 ± 0.08	0.30 ± 0.05	0.24 ± 0.09	12	68	18	0.999	**0.011**	**0.043**
L/R medullary reticularis formation	0.28 ± 0.09	0.36 ± 0.08	0.31 ± 0.08	3	25	12	0.324	**0.002**	0.220
L/R Pendunculopontine Nucleus	0.34 ± 0.09	0.42 ± 0.06	0.35 ± 0.11	20	59	34	0.999	**0.002**	**0.032**
L/R Dorsal raphe nuclei	0.29 ± 0.07	0.35 ± 0.04	0.30 ± 0.09	24	93	26	0.999	**<0.001**	**0.040**
L/R Locus coeruleus	0.29 ± 0.09	0.37 ± 0.05	0.30 ± 0.10	21	35	60	0.999	**<0.001**	**0.009**
L/R Medulla	0.17 ± 0.07	0.36 ± 0.08	0.20 ± 0.10	200	598	33	0.345	**<0.001**	**0.022**
R Substantia nigra	0.38 ± 0.06	0.44 ± 0.06	0.37 ± 0.07	20	60	33	0.999	**0.002**	**0.009**
R Red nucleus	0.31 ± 0.08	0.36 ± 0.07	0.29 ± 0.07	13	60	22	0.999	**0.034**	**0.026**
FA white matter tracts									
L Corticospinal tract	0.36 ± 0.05	0.42 ± 0.04	0.39 ± 0.07	812	3,261	25	0.166	**<0.001**	0.138
L Uncinate fasciculus	0.28 ± 0.05	0.31 ± 0.03	0.29 ± 0.05	78	778	10	0.324	**0.006**	0.555
L Superior cerebellar peduncle	0.30 ± 0.10	0.37 ± 0.04	0.31 ± 0.11	28	86	33	0..999	**0.004**	**0.021**
L Inferior cerebellar peduncle	0.26 ± 0.07	0.34 ± 0.06	0.29 ± 0.07	30	79	38	0.182	**<0.001**	0.086
L Tapetum	0.26 ± 0.08	0.23 ± 0.06	0.19 ± 0.06	21	45	47	**<0.001**	0.194	0.147
L/R corpus callosum body	0.36 ± 0.06	0.31 ± 0.04	0.32 ± 0.06	226	1,279	18	**0.011**	**0.002**	0.999
L/R middle cerebellar peduncle	0.34 ± 0.06	0.42 ± 0.05	0.37 ± 0.08	695	1,402	50	0.273	**<0.001**	0.071
L/R Corpus callosum splenium	0.47 ± 0.05	0.44 ± 0.03	0.42 ± 0.07	269	1,166	23	**0.004**	**0.002**	0.999
R Anterior thalamic radiation	0.31 ± 0.04	0.33 ± 0.03	0.32 ± 0.03	428	4,248	10	0.411	**0.012**	0.591
R Corticospinal tract	0.38 ± 0.04	0.42 ± 0.03	0.41 ± 0.05	776	3,365	23	**0.036**	**0.002**	0.999
R Inferior cerebellar peduncle	0.26 ± 0.07	0.34 ± 0.06	0.29 ± 0.07	40	78	51	0.441	**<0.001**	**0.030**
R Superior longitudinal fasciculus	0.35 ± 0.03	0.35 ± 0.03	0.37 ± 0.04	593	8,401	7	**0.006**	0.927	0.125

Table 2. Continued

Region	HC (mean ± SD)	RBD (mean ± SD)	PD (mean ± SD)	Cluster (voxel)	ROI (voxel)	Ratio (%)	P (corrected) PD vs. HC	RBD vs. HC	RBD vs. PD
R Superior longitudinal fasciculus temporal	0.38 ± 0.04	0.42 ± 0.04	0.41 ± 0.04	38	330	12	0.052	***0.006***	0.999
R Superior cerebellar peduncle	0.26 ± 0.10	0.34 ± 0.04	0.26 ± 0.11	18	80	23	0.999	***0.003***	***0.008***
R Uncinate fasciculus	0.26 ± 0.04	0.28 ± 0.04	0.29 ± 0.03	73	792	9	***0.006***	0.723	0.221
R Tapetum	0.28 ± 0.08	0.23 ± 0.07	0.22 ± 0.07	26	48	54	***0.010***	0.058	0.999

TBM, Tensor-based morphometry; HC, healthy controls; RBD, REM sleep behavior disorder; PD, Parkinson's disease; Cluster, contiguous voxels per ROI exhibiting significantly different values across groups; ROI, Atlas-based predefined ROI (for details, see Methods); L, left; R, right; Ratio, cluster voxel/ROI voxel*100; FA, fractional anisotropy; Log-Jacobian values were multiplied by 100 for better visualization; significant *p*-values are printed in bold italics.

meaningful variation of UPDRS scores. Thus, we restricted these analyses to the latter group, and only included brain regions that showed significantly different values as compared with HC. We observed an inverse correlation of FA in the right corticospinal tract with UPDRS III scores in the PD group ($r = -0.439$, $p < 0.04$).

Discussion

We observed convergent patterns of structural and microstructural brain changes in multiple cortical and subcortical regions in a cohort of RBD and PD individuals compared with HC. Whereas RBD subjects showed distinct elevations of FA mainly in the BS, volume loss in the basal ganglia was specific to PD individuals. However, both RBD and PD subjects showed similar microstructural alterations in major cerebral motor and non-motor pathways. Moreover, we provide evidence that RBD individuals exhibit structural brain alterations that may be compensatory in nature.

We found altered volume and microstructural integrity in several BS regions commonly associated with RBD and PD pathology in the disease groups. Specifically, RBD patients showed increased FA in various BS and midbrain regions involved in RBD pathophysiology such as the raphe nuclei, LC, and medulla oblongata. Only few DTI studies involving RBD subjects are available, providing incongruent results. Unger et al. reported decreased FA in the rostral pons and midbrain of RBD indivduals [8], whereas others have found normal FA values in these regions [9]. Reductions of FA in white matter regions are believed to reflect axonal damage and demyelination [28]. The meaning of increased FA in both white matter and gray matter regions on the other hand is less clear. For example, increased FA within white matter tracts can reflect either a real gain of myelination or number of axons, but also a loss of dendrite sprouting [28]. Increased FA has also been observed in cortical lesions in patients with multiple sclerosis. The authors discussed a loss of dendrites, glial cell activation, and neuronal damage as possible causes [29]. In light of these reports and common concepts of RBD pathology [1], the increases of FA observed in key BS regions are likely reflecting neurodegeneration. RBD individuals also showed higher FA in these regions as compared with PD individuals, and the latter group did not show any differences of BS FA as compared with HC. This observation suggests that these changes are specific to RBD, but may not be a consistent feature in PD patients. In contrast, PD patients showed lower than normal volume of the substantia nigra, PPN, and a trend level reduction of LC volume. All three regions are known to be affected in PD, and neuroimaging studies have reported altered microstructural integrity in PD individuals [28, 30, 31]. These findings were not apparent in RBD individuals, suggesting these changes are associated with more advanced PD pathology.

Contrary to our finding of higher caudate volume in RBD individuals compared with HC, reduced striatal volumes in RBD patients compared with both early PD individuals and HC have been reported previously [11], and volume reductions were pronounced in subjects with concurrent cognitive deficits [32]. The caudate nucleus predominantly projects to frontal cortical regions, and has been associated with cognitive function in both health and neurodegenerative diseases [33]. The cause of higher caudate volume in RBD individuals is not clear, but may represent a temporary compensatory mechanism to maintain intact executive functioning that eventually breaks down with manifesting PD pathology. In line with our observation, the majority of previous studies found reduced putaminal volumes in PD, likely reflecting nigrostriatal degeneration [34, 35].

We observed higher thalamic volume in PD individuals compared with HC, and to a lesser extent, to RBD individuals. Even though a precise anatomical allocation within the thalamic inner structure is limited at 3T, the utilization of a histopathology-based MRI atlas published by Xao et al. [36] suggested that the cluster identified resided in the dorsolateral portion of the thalamus, encompassing the anterior nuclear group and the ventral anterior nucleus. The latter nucleus is considered a major relay node in striato-cortical circuitry, whereas the anterior nuclei are part of the "limbic" thalamus involved in memory function receiving afferent projections from the hippocampus [37]. We speculate the thalamic structural changes observed may be a consequence of altered limbic and striatal input. Congruent with our findings, increased gray matter volume in similar thalamic regions in PD has been reported previously [38].

RBD individuals showed increased volume in both non-motor and motor cerebellar regions, and the cerebellar white matter compared with HC. Interestingly, cerebellar white matter volume was also substantially higher in RBD compared with PD individuals, whereas PD subjects showed cerebellar volume loss compared with HC. These findings were corroborated by DTI showing elevated FA values in RBD individuals in the cerebellar peduncles compared with both HC and PD patients. Prior imaging findings on the structural integrity of the CER in RBD are controversial. Whereas some authors reported reduced volume compared with HC [10], others have found increased cerebellar gray matter volume [39]. Moreover, a recent FDG (^{18}F-fluorodeoxyglucose) PET study reported relative cerebellar hypermetabolism in RBD subjects suggesting a compensatory overactivation [7]. In line with the latter observation, the cerebellar volume increase in RBD subjects compared with both HC

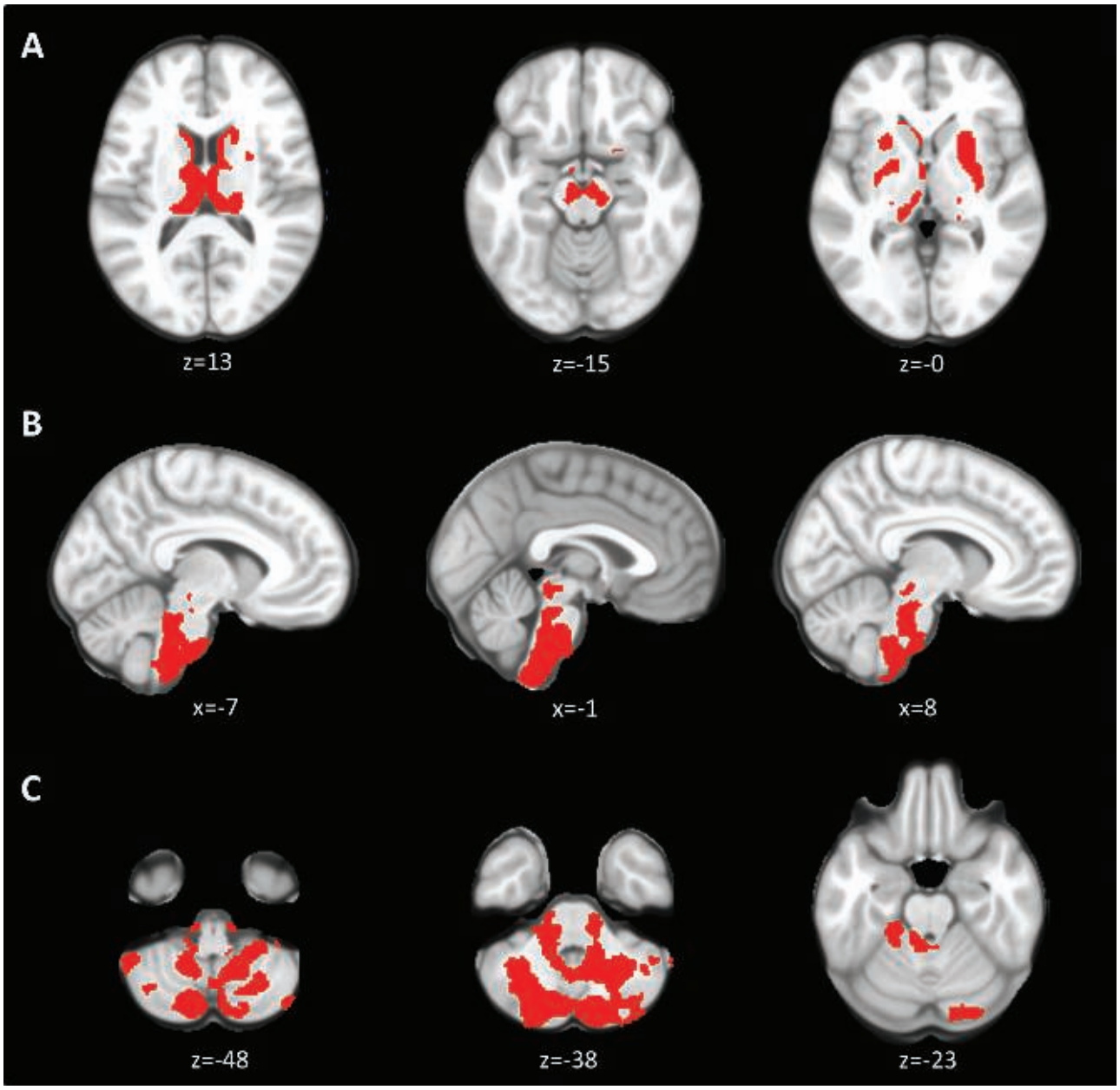

Figure 1. Regions showing differences of volume across groups on TBM analysis. (A) A significant difference of volume across groups (HC, RBD, and PD) was observed in the bilateral thalamus (left panel), midbrain, including the substantia nigra (middle panel), bilateral putamen, bilateral globus pallidum, and the right caudate nucleus (right panel). (B) Voxels displaying a significant difference of volume across groups in the BS. (C) Cerebellar regions exhibiting significantly different volume across groups, including lobules I–V, VIIb, VIIIa/b, IX. X, Crus I/II, cerebellar vermis, and the cerebellar white matter. For details on the direction of the changes observed and pairwise group comparisons, please see Table 2 and Figure 2. The clusters displayed were significant at $p < 0.05$, corrected. Coordinates are displayed in Montreal Neurological Institute (MNI) standard space. TBM, tensor-based morphometry; HC, healthy controls; RBD, rapid eye movement sleep behavior disorder; PD, Parkinson's disease.

and PD patients observed in our study hints to a compensatory mechanism in RBD that eventually fails as neurodegeneration progresses.

PD patients exhibited above normal FA values in the corticospinal tract. Elevations of FA in the pyramidal tract have consistently been reported in PD, and have been suggested to either reflect a compensatory increase in axonal density as a response to reduced dopaminergic input to cortico-basal-ganglia-thalamo-cortical circuitry, or to depict a loss of dendritic branching as a consequence of neurodegeneration [40]. In fact, these two hypotheses do not have to be mutually exclusive. Along these lines, we did observe an inverse correlation of FA in the right corticospinal tract with UPDRS III scores in PD subjects. However, RBD patients with normal motor function displayed similar elevations of FA in the corticospinal tracts. Furthermore, increased FA in both RBD and PD patients was also observed in fiber tracts such as the uncinate and superior longitudinal fasciculi that primarily are related to non-motor functions [41, 42], and there was no correlation of FA and motor measures in the latter tracts. These observations suggest the co-occurrence of neurodegenerative processes and compensatory mechanisms in the cerebral white matter of RBD and PD subjects.

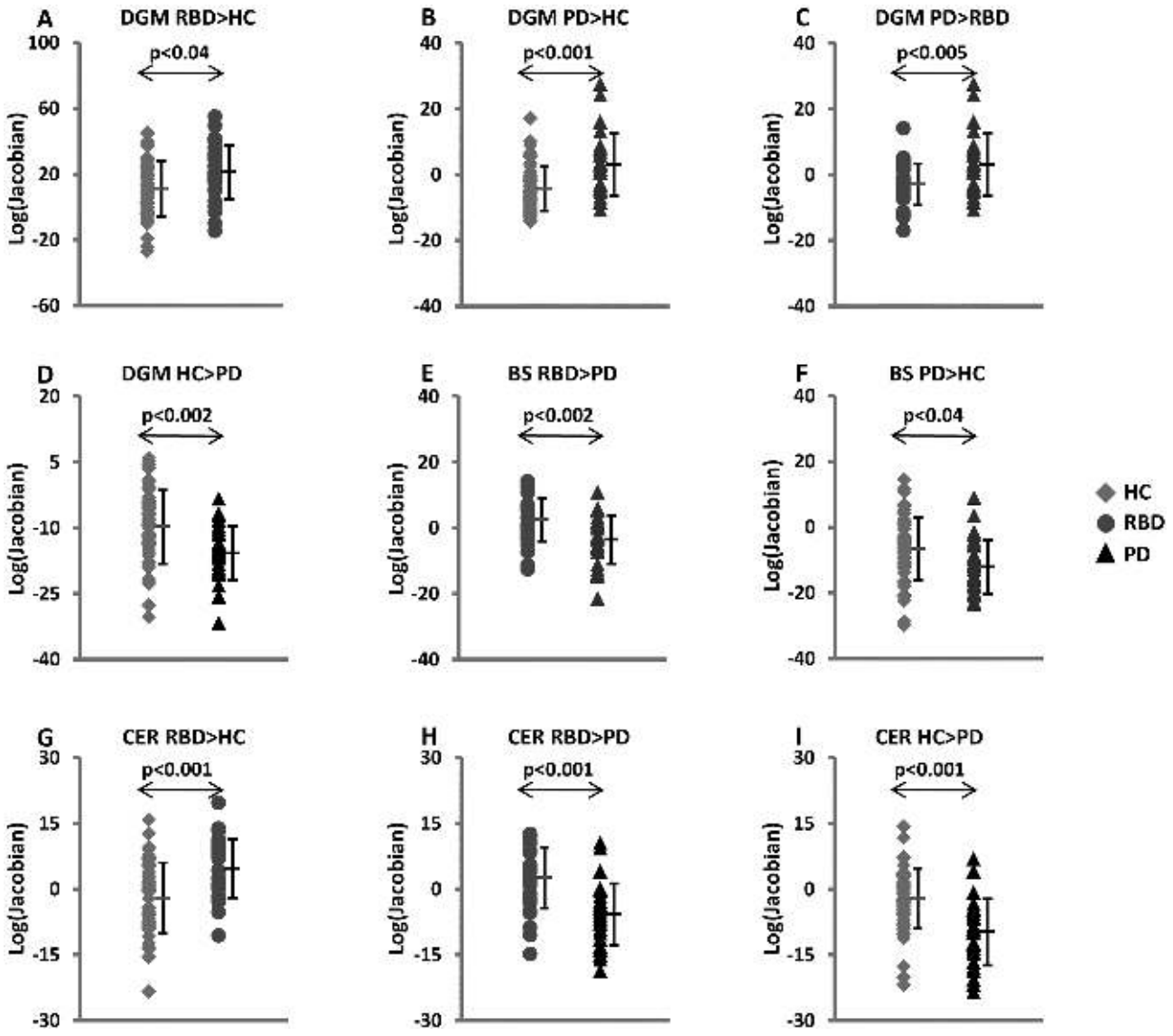

Figure 2. Post hoc plots of pairwise comparisons of significant TBM clusters. (A) RBD individuals showed higher volume of the right caudate nucleus compared with HC. Thalamic volume was larger in PD individuals compared with their RBD counterparts (B) and to HC (C), respectively. (D) PD subjects exhibited lower volume compared with HC in the bilateral globus pallidum, putamen, and in the substantia nigra. (E) RBD subjects showed higher volume compared with PD patients in the pons, medulla oblongata, including the medullary reticularis formation, and the locus coeruleus. (F) Volume of the PPN was significantly lower in PD patients compared with HC. (G) RBD patients showed higher volume of the anterior and posterior CER compared with HC. (H) Similarly, cerebellar gray and white matter volume was larger in RBD compared with PD patients. (I) Lastly, PD patients showed lower cerebellar volume in several lobules in both the anterior and posterior CER compared with HC. For improved clarity, individual values of subregions (please see Table 2) comprising the higher level ROI (DGM, BS, and CER) that showed parallel and significant differences on pairwise comparisons between groups (HC, RBD, and PD) were averaged. Bonferroni tests for all regions are displayed in Table 2.

Conversely, we found lower than normal FA in the corpus callosum of RBD and PD individuals, respectively. Reduced callosal FA has been reported by a recent meta-analysis including more than 1,000 PD patients, and has been associated with cognitive dysfunction, but also gait disturbances [28]. It is also known that agenesis of the corpus callosum impacts sleep architecture, causing an increase of REM sleep episodes [43], and structural connectivity of the corpus callosum has been found to be reduced in PD patients with concurrent RBD [44]. However, current concepts of RBD pathophysiology do not include the corpus callosum [1].

In contrast to prior reports of significant cortical atrophy in both RBD [45] and PD [46], we did not observe significant cortical thinning in either group. The most likely explanation for this discrepancy is the intact cognitive status of all subjects included in our study. Indeed, studies on both RBD and PD individuals have demonstrated that cortical thinning was most pronounced in subjects with cognitive deficits [32, 47].

There are limitations to our study. First, the presence of RBD was not systematically assessed in the PD cohort. There is evidence of a distinct clinical phenotype and less favorable outcome of PD-RBD+ patients compared with their RBD– counterparts [48], and imaging studies have shown structural brain differences between PD-RBD+ and PD-RBD– patients in subcortical and cortical areas [49]. Moreover, even though the vast majority of RBD patients go on to eventually convert to PD or another alpha-synucleinopathy, some do not, questioning the hypothesis of RBD unequivocally constituting a prodromal state of progressive

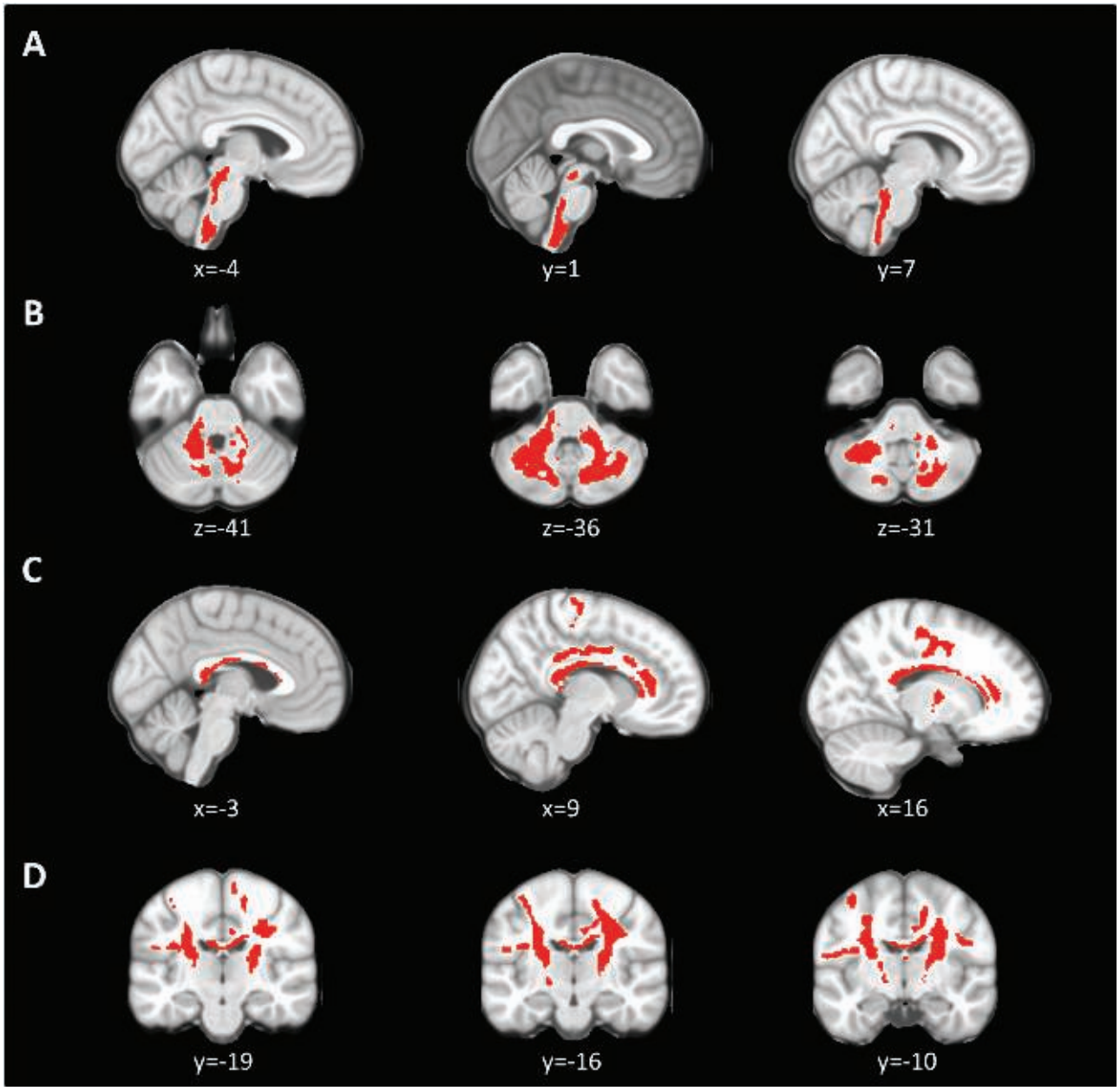

Figure 3. Regions showing altered FA across groups on DTI. (A) Differences of FA across groups (HC, RBD, and PD) were observed in the BS and midbrain. (B) FA differed across groups in the bilateral inferior, middle, and superior peduncles. (C) Altered FA across groups was observed in the corpus callosum. (D) We found significant alterations of FA across groups in several major motor and non-motor white matter pathways, including the bilateral corticospinal tracts. For details on the direction of the changes observed and pairwise group comparisons, please see Table 2 and Figure 4. The clusters displayed were significant at $p < 0.05$, corrected. Coordinates are displayed in MNI standard space. TBM, tensor-based morphometry; HC, healthy controls; RBD, rapid eye movement sleep behavior disorder; PD, Parkinson's disease.

neurodegeneration [3]. Furthermore, a minority of PD patients develop RBD symptoms only years after motor manifestation [3]. This phenomenon may rely on differences in the chronological order of incipient neurodegeneration in anatomically closely related BS and midbrain regions in PD, but does not necessarily imply a distinct neurodegenerative process in "RBD negative" PD as compared with PD with preceding RBD [50]. Along these lines, we have previously found that an abnormal RBD-specific metabolic brain network was expressed at equally elevated levels in PD patients independent of their RBD status [7].

Second, this study is cross-sectional and retrospective, and we do not know if and when any of the RBD subjects will develop PD or another alpha-synucleinopathy. Thus, our results have to be interpreted with caution, and longitudinal studies involving larger samples are warranted to confirm our findings.

Lastly, due to the retrospective nature of this study, and the marked male predominance in RBD [51], we were not able to achieve perfect gender-matching of HC to both the RBD and PD cohorts, respectively. However, gender was entered as a variable of no interest into all analyses. Importantly, we did control for age which likely has a much greater impact on our analyses [52]. It is a strength of our study that we rigorously controlled for cognitive dysfunction, and applied a strict motor threshold to RBD

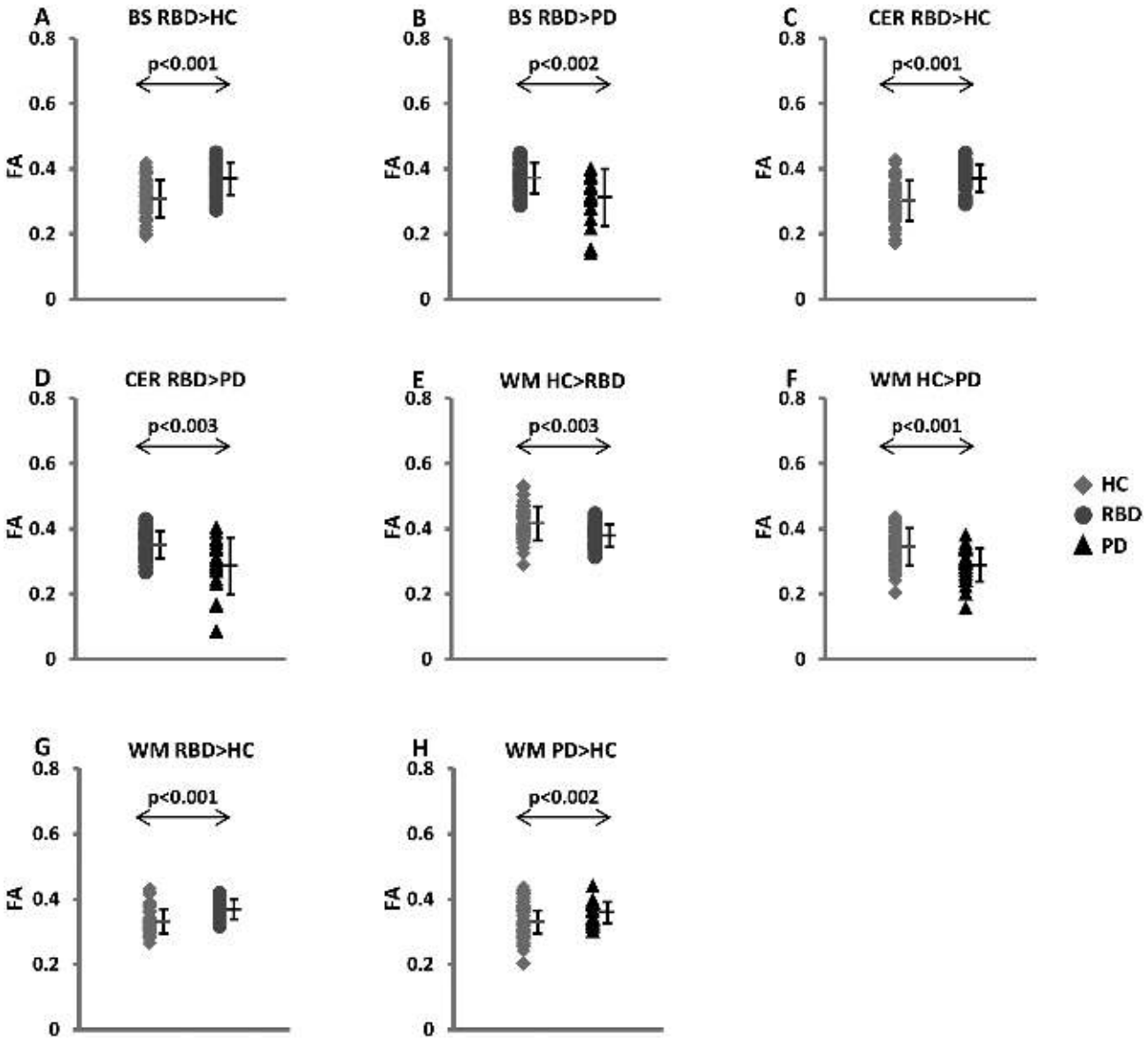

Figure 4. Post hoc plots of pairwise comparisons of significant FA clusters. In the BS, RBD individuals showed higher FA compared with both HC (A) and PD subjects (B). (C) RBD subjects displayed significantly higher FA in the superior, middle, and inferior cerebellar peduncles. (D) Similarly, FA in RBD individuals was increased compared with PD subjects in both superior cerebellar peduncles, and the right inferior cerebellar peduncle. FA in the corpus callosum was significantly lower in HC compared with both RBD (E) and PD individuals (F). (G) In contrast, RBD individuals showed higher than normal FA in several cerebral white matter tracts, including the corticospinal tracts, right anterior thalamic radiation, right superior longitudinal fasciculus, and left uncinate fasciculus. (I) Similar FA elevations were observed in the right corticospinal tract, right superior longitudinal fasciculus, and right uncinate fasciculus of PD individuals compared with HC. For improved clarity, individual values of subregions (please see Table 2) comprising the higher level ROI (BS, cerebral white matter, and CER) that showed parallel and significant differences on pairwise comparisons between groups (HC, RBD, and PD) were averaged. Bonferroni tests for all regions are displayed in Table 2.

individuals to ensure that none showed any signs suspicious of emerging parkinsonism.

In conclusion, we identified convergent patterns of structural and microstructural brain changes in a cohort of RBD and PD patients compared with HC. We speculate that the changes observed reflect both neurodegenerative processes and compensatory mechanisms for declining nigro-striatal dopaminergic integrity and spreading of alpha-synuclein pathology. Alongside common structural brain alterations, we identified RBD-specific changes in the BS that were not apparent in the PD cohort. The latter finding may reflect a certain heterogeneity of RBD pathophysiology, supported by the notion that some RBD individuals never phenoconvert to PD, or eventually develop another alpha-synucleinopathy such as multiple system atrophy or Lewy body dementia. Our results imply that a multimodal imaging approach allocates complimentary information on the underlying pathophysiological relationship of RBD and PD, and is superior to single modality analyses. This study further strengthens the hypothesis of RBD constituting a prodromal stage of progressive neurodegeneration, and PD in particular.

Acknowledgments

We thank all patients and controls who participated in this study. We thank Shahram Mirzazade for the technical help with

the MRI measurements in Aachen. Brain normalizations were performed with computing resources granted by RWTH Aachen University under project rwth0212. Data used in the preparation of this article were obtained from the PPMI database (www.ppmi-info.org/data). For up-to-date information on the study, visit www.ppmi-info.org. PPMI—a public–private partnership—is funded by the Michael J. Fox Foundation for Parkinson's Research and funding partners, including AbbVie, Allergan, Avid Radiopharmaceuticals, Biogen Idec, BioLegend, Bristol-Myers Squibb, Celgene, Denali, GE Healthcare, Genentech, GlaxoSmithKline, Lilly, Lundbeck, Merck, MSD, Pfizer Inc., Piramal, Prevail Therapeutics, Roche CNS group, Sanofi Genzyme, Servier, Takeda, Teva, UCB, Verily, Voyager Therapeutics, and Golub Capital.

Funding

K.R. and parts of this project were funded by the German Federal Ministry of Education and Research (BMBF 01GQ1402). This work was further supported by a Research Grant from the Faculty of Medicine, RWTH Aachen University (IZKF, 124/16) and the International Research Training Group (IRTG 2150) of the German Research Foundation (DFG). WHO and part of this project were supported by the ParkinsonFonds Deutschland, Berlin, Germany.

Financial disclosure: Nothing to disclose.

Non-financial disclosure: The authors report no conflict of interest.

References

1. Boeve BF, *et al*. Pathophysiology of REM sleep behaviour disorder and relevance to neurodegenerative disease. *Brain*. 2007;**130**(Pt 11):2770–2788.
2. Postuma RB, *et al*. Risk and predictors of dementia and parkinsonism in idiopathic REM sleep behaviour disorder: a multicentre study. *Brain*. 2019;**142**(3):744–759.
3. Högl B, *et al*. Idiopathic REM sleep behaviour disorder and neurodegeneration—an update. *Nat Rev Neurol*. 2018;**14**(1):40–55.
4. Heller J, *et al*. Brain imaging findings in idiopathic REM sleep behavior disorder (RBD)—a systematic review on potential biomarkers for neurodegeneration. *Sleep Med Rev*. 2017;**34**:23–33.
5. Iranzo A, *et al*. Serial dopamine transporter imaging of nigrostriatal function in patients with idiopathic rapid-eye-movement sleep behaviour disorder: a prospective study. *Lancet Neurol*. 2011;**10**(9):797–805.
6. Holtbernd F, *et al*. Abnormal metabolic network activity in REM sleep behavior disorder. *Neurology*. 2014;**82**(7):620–627.
7. Meles SK, *et al*. The metabolic pattern of idiopathic REM sleep behavior disorder reflects early-stage Parkinson disease. *J Nucl Med*. 2018;**59**(9):1437–1444.
8. Scherfler C, *et al*. White and gray matter abnormalities in idiopathic rapid eye movement sleep behavior disorder: a diffusion-tensor imaging and voxel-based morphometry study. *Ann Neurol*. 2011;**69**(2):400–407.
9. Unger MM, *et al*. Diffusion tensor imaging in idiopathic REM sleep behavior disorder reveals microstructural changes in the brainstem, substantia nigra, olfactory region, and other brain regions. *Sleep*. 2010;**33**(6):767–773.
10. Hanyu H, *et al*. Voxel-based magnetic resonance imaging study of structural brain changes in patients with idiopathic REM sleep behavior disorder. *Parkinsonism Relat Disord*. 2012;**18**(2):136–139.
11. Ellmore TM, *et al*. Reduced volume of the putamen in REM sleep behavior disorder patients. *Parkinsonism Relat Disord*. 2010;**16**(10):645–649.
12. Hughes AJ, *et al*. Accuracy of clinical diagnosis of idiopathic Parkinson's disease: a clinico-pathological study of 100 cases. *J Neurol Neurosurg Psychiatry*. 1992;**55**(3):181–184.
13. American Academy of Sleep Medicine. *International Classification of Sleep Disorders*. 3rd ed. Darien, IL: American Academy of Sleep Medicine; 2014.
14. Nasreddine ZS, *et al*. The Montreal Cognitive Assessment, MoCA: a brief screening tool for mild cognitive impairment. *J Am Geriatr Soc*. 2005;**53**(4):695–699.
15. Fahn S, Elton R. Unified Parkinson's disease rating scale. In: Fahn S, Goldstein M, Marsden CD, Calne DB, eds. *Recent Developments in Parkinson's Disease. Vol. 2*. New Jersey: MacMillan; 1987: 153–163.
16. Schiess MC, *et al*. Parkinson's disease subtypes: clinical classification and ventricular cerebrospinal fluid analysis. *Parkinsonism Relat Disord*. 2000;**6**(2):69–76.
17. Goetz CG, *et al*. Movement Disorder Society-sponsored revision of the Unified Parkinson's Disease Rating Scale (MDS-UPDRS): process, format, and clinimetric testing plan. *Mov Disord*. 2007;**22**(1):41–47.
18. Folstein MF, *et al*. "Mini-mental state". A practical method for grading the cognitive state of patients for the clinician. *J Psychiatr Res*. 1975;**12**(3):189–198.
19. Avants B, Tustison N. *ANTs/ANTsR brain templates*. Figshare. Dataset. https://doi.org/10.6084/m9.figshare.915436.v2, 2018.
20. Tustison NJ, *et al*. Large-scale evaluation of ANTs and FreeSurfer cortical thickness measurements. *Neuroimage*. 2014;**99**:166–179.
21. Hua X, *et al*. Tensor-based morphometry as a neuroimaging biomarker for Alzheimer's disease: an MRI study of 676 AD, MCI, and normal subjects. *Neuroimage*. 2008;**43**(3):458–469.
22. Tustison NJ, *et al*. Logical circularity in voxel-based analysis: normalization strategy may induce statistical bias. *Hum Brain Mapp*. 2014;**35**(3):745–759.
23. Eklund A, *et al*. BROCCOLI: software for fast fMRI analysis on many-core CPUs and GPUs. *Front Neuroinform*. 2014;**8**:24.
24. Mori S, *et al*. Stereotaxic white matter atlas based on diffusion tensor imaging in an ICBM template. *Neuroimage*. 2008;**40**(2):570–582.
25. Diedrichsen J. A spatially unbiased atlas template of the human cerebellum. *Neuroimage*. 2006;**33**(1):127–138.
26. Edlow BL, *et al*. Neuroanatomic connectivity of the human ascending arousal system critical to consciousness and its disorders. *J Neuropathol Exp Neurol*. 2012;**71**(6):531–546.
27. Tang Y, *et al*. A probabilistic atlas of human brainstem pathways based on connectome imaging data. *Neuroimage*. 2018;**169**:227–239.
28. Atkinson-Clement C, *et al*. Diffusion tensor imaging in Parkinson's disease: Review and meta-analysis. *Neuroimage Clin*. 2017;**16**:98–110.
29. Filippi M, *et al*. Diffusion tensor imaging and functional MRI. *Handb Clin Neurol*. 2016;**136**:1065–1087.
30. Youn J, *et al*. Alterations of mean diffusivity of pedunculopontine nucleus pathway in Parkinson's disease patients with freezing of gait. *Parkinsonism Relat Disord*. 2015;**21**(1):12–17.

31. Liu KY, *et al*. Magnetic resonance imaging of the human locus coeruleus: a systematic review. *Neurosci Biobehav Rev*. 2017;**83**:325–355.
32. Rahayel S, *et al*. Cortical and subcortical gray matter bases of cognitive deficits in REM sleep behavior disorder. *Neurology*. 2018;**90**(20):e1759–e1770.
33. Grahn JA, *et al*. The cognitive functions of the caudate nucleus. *Prog Neurobiol*. 2008;**86**(3):141–155.
34. Sterling NW, *et al*. Striatal shape in Parkinson's disease. *Neurobiol Aging*. 2013;**34**(11):2510–2516.
35. Kish SJ, *et al*. Uneven pattern of dopamine loss in the striatum of patients with idiopathic Parkinson's disease. Pathophysiologic and clinical implications. *N Engl J Med*. 1988;**318**(14):876–880.
36. Xiao Y, *et al*. Multi-contrast unbiased MRI atlas of a Parkinson's disease population. *Int J Comput Assist Radiol Surg*. 2015;**10**(3):329–341.
37. Wolff M, *et al*. Functional heterogeneity of the limbic thalamus: From hippocampal to cortical functions. *Neurosci Biobehav Rev*. 2015;**54**:120–130.
38. Chen Y, *et al*. The morphology of thalamic subnuclei in Parkinson's disease and the effects of machine learning on disease diagnosis and clinical evaluation. *J Neurol Sci*. 2020;**411**:116721.
39. Chen M, *et al*. Structural and functional brain alterations in patients with idiopathic rapid eye movement sleep behavior disorder. *J Neuroradiol*. 2020 [Epub ahead of print].
40. Mole JP, *et al*. Increased fractional anisotropy in the motor tracts of Parkinson's disease suggests compensatory neuroplasticity or selective neurodegeneration. *Eur Radiol*. 2016;**26**(10):3327–3335.
41. Von Der Heide RJ, *et al*. Dissecting the uncinate fasciculus: disorders, controversies and a hypothesis. *Brain*. 2013;**136**(Pt 6):1692–1707.
42. Wang X, *et al*. Subcomponents and connectivity of the superior longitudinal fasciculus in the human brain. *Brain Struct Funct*. 2016;**221**(4):2075–2092.
43. Nielsen T, *et al*. Sleep architecture in agenesis of the corpus callosum: laboratory assessment of four cases. *J Sleep Res*. 1992;**1**(3):197–200.
44. Ghazi Sherbaf F, *et al*. Microstructural changes in patients with Parkinson's disease comorbid with REM sleep behaviour disorder and depressive symptoms. *Front Neurol*. 2018;**9**:441.
45. Pereira JB, *et al*. Cortical thinning in patients with REM sleep behavior disorder is associated with clinical progression. *NPJ Parkinsons Dis*. 2019;**5**:7.
46. Sarasso E, *et al*. Progression of gray and white matter brain damage in Parkinson's disease: a critical review of structural MRI literature. *J Neurol*. 2020 [Epub ahead of print].
47. Danti S, *et al*. Cortical thickness in de novo patients with Parkinson disease and mild cognitive impairment with consideration of clinical phenotype and motor laterality. *Eur J Neurol*. 2015;**22**(12):1564–1572.
48. Ferri R, *et al*. The timing between REM sleep behavior disorder and Parkinson's disease. *Sleep Breath*. 2014;**18**(2):319–323.
49. Boucetta S, *et al*. Structural brain alterations associated with rapid eye movement sleep behavior disorder in Parkinson's disease. *Sci Rep*. 2016;**6**:26782.
50. Lai YY, *et al*. Physiological and anatomical link between Parkinson-like disease and REM sleep behavior disorder. *Mol Neurobiol*. 2003;**27**(2):137–152.
51. Ju YE. Rapid eye movement sleep behavior disorder in adults younger than 50 years of age. *Sleep Med*. 2013;**14**(8):768–774.
52. Grajauskas LA, *et al*. MRI-based evaluation of structural degeneration in the ageing brain: pathophysiology and assessment. *Ageing Res Rev*. 2019;**49**:67–82.